Modeling an Integral Dual Solar/Gas-Fired Generator for a Water-Lithium Bromide Absorption Chiller

J. Cao
Assoc. Mem. ASME

R. N. Christensen
Mem. ASME

Department of Mechanical Engineering,
The Ohio State University,
Columbus, OH 43210

This paper presents a design procedure for a dual solar/gas-fired generator of an absorption chiller. The solar energy is the primary driving source for the generator, while the natural gas serves as the backup heat when the solar energy is unavailable or insufficient. Saturated forced convective boiling for binary mixtures has been considered to account for the reduction in the heat transfer coefficient observed for most mixtures. The simultaneous solar and gas-fired desorption process was investigated. The generator constructed based on modeling results yielded good performance in the experiment.
[S0195-0738(00)00704-4]

Introduction

Absorption chillers using water-lithium bromide have been recognized as one of the most promising competitors to the vapor compression chillers that currently dominate the market. Absorption cycles have some advantages which explain the resurgence of interest in their development. The working fluids in absorption cycles are environmentally benign compared to the ozone-depleting chlorofluorocarbons (CFCs), hydrochlorofluorocarbons (HCFCs), or hydrofluorocarbon (HFCs) used in the vapor compression cycles. The Montreal Protocol and its Copenhagen Amendment required the cessation of production of CFCs by January 1, 1996, and complete cessation of the production of HCFCs by January 1 [1]. The U.S. Department of Energy (DOE), manufacturers, and utilities have invested millions of dollars in research and development of absorption air conditioning systems [2]. Another advantage of absorption machines is that they potentially provide higher primary energy efficiency than vapor compression chillers. The use of natural gas or solar energy as the driving energy also reduces the demand for electricity, which would lessen the peak electric demand due to summer cooling loads. Water-lithium bromide absorption systems have a reputation for consistent, reliable service and low operational cost. The choice between vapor compression refrigeration (VCR) and absorption refrigeration (AR) depends strongly on economic factors and environmental considerations.

The objective of this paper is to develop a design model for an integral dual-fired generator that has the capability of utilizing solar energy and natural gas as the driving energies separately or simultaneously. A parametric analysis is also performed to study the effects of varying solar fluid inlet temperature and flow rate on the heat exchanger performance. Prior to developing an integral solar/gas-fired generator model, the cycle thermodynamic state points have to be specified. This has been accomplished through cycle modeling [3].

Component Description

The generator has 50 fluted tubes installed vertically in the space between two concentric tubes; see Fig. 1. The water-lithium bromide mixture flows upward around the fluted tubes, while the solar fluid (10 percent water-glycol in this case) enters the fluted tubes from the top of the generator. The flue gas resulting from combustion with roughly 25–30 percent excess air will reach about 1650°C. It flows upward through the gap between a ceramic insert and the smaller cylindrical tube. The stainless steel rectangular-shaped fins are used in the gap to enhance heat transfer. However, they cannot be placed immediately after the burner since the carbon steel or stainless steel will lose its material strength under high temperature. The rectangular fins are brazed onto the inner surface of the smaller cylindrical tube after a certain flow length such that the fin tip temperature is low enough to prevent structural damage. The rectangular fins have the advantages of low cost, ease of manufacture and brazing, and low pressure loss. The flue gas and the water-lithium bromide solution are in co-current flow, while the solar fluid and the water-lithium bromide solution are in countercurrent flow. The outer diameters of concentric tubes surrounding the fluted tubes are 0.2286 and 0.2794 m. The dimensions of the fluted tubes are listed in Table 1, and the rectangular fin geometry is given in Table 2. Figure 2

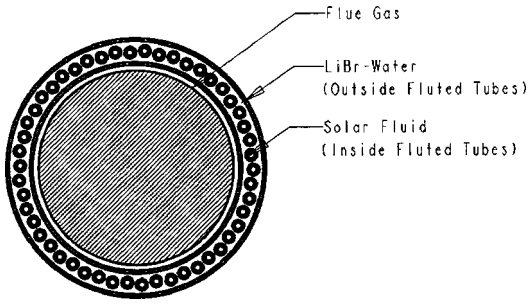

Fig. 1 Top view of the generator

Table 1 Fluted tube dimensions

D_{eo} (m)	D_{bi} (m)	Thickness t_w (m)	N_s	Pitch p (m)
0.01262	0.00706	4.064×10^{-4}	4	0.00564

Table 2 Rectangular fin dimensions

Fin Height (m)	Thickness (m)	Pitch (m)
0.00635	6.096×10^{-4}	0.003175

Contributed by the Advanced Energy Systems Division and presented at the International Mechanical Engineering Congress & Exposition, the Winter Annual Meeting, Nashville, Tennessee, November 14–19, 1999, of THE AMERICAN SOCIETY OF MECHANICAL ENGINEERS. Manuscript received by the AES Division, December 9, 1999; revised manuscript received July 10, 2000. Associate Technical Editor: D. L. O'Neal.

Downloaded From: https://energyresources.asmedigitalcollection.asme.org on 06/28/2019 Terms of Use: http://www.asme.org/about-asme/terms-of-use

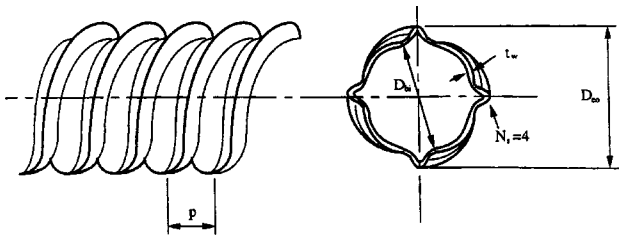

Fig. 2 Spirally fluted tube parameters

Table 3 Thermodynamic state points of the generator

	inlet	outlet
solution temperature (°C)	128.3	154.4
solution concentration	0.578	0.610
liquid mass flow rate (kg/s)	0.3251	0.3085
vapor mass flow rate (kg/s)	0	0.0165
solar fluid temperature (°C)	170	163
solar fluid flow rate (kg/s)	2.0488	2.0488
flue gas temperature (°C)	1648	varying
flue gas flow rate (kg/s)	0.03415	0.03415

gives the geometry of a fluted tube. The thermodynamic state points of the generator are presented in Table 3 for firing by either the solar fluid or the natural gas.

Analysis

The water-lithium bromide solution enters the generator as subcooled liquid, is heated until it reaches saturation and then the solution undergoes desorption. Two regions are identified according to the heat transfer mechanism:

I Subcooled liquid region: In this region, the water-lithium bromide solution temperature and the wall temperature are below saturation temperature at the given pressure and inlet concentration. This region is treated as single phase heat transfer.

II Saturated boiling: In this region, the wall temperature is higher than the bulk solution temperature. The water-lithium bromide liquid and vapor are in co-current flow. Analysis based on the superficial velocities (i.e., volumetric fluxes) of liquid and vapor indicates that the flow pattern is most likely in the slug flow [4]. This region is modeled as saturated boiling. However, binary mixture forced convective boiling is different from pure component boiling, in that a significant reduction in the heat transfer coefficient is observed for mixtures which is attributable to mass transfer and Prandtl number effects. Bennett and Chen [5] proposed a correlation that incorporates mass transfer effects on both microscopic heat transfer and macroscopic heat transfer. For microscopic heat transfer, they postulated that the thermal driving potential—effective superheat—is reduced for binary mixtures and could be represented by combining Forster-Zuber's pool boiling model and Florshuetz-Khan's vapor bubble interfacial temperature analysis. The result is that a suppression factor is introduced for binary mixtures in addition to the suppression factor for single-component fluids. For macroscopic heat transfer, it is assumed that the vapor is generated in equilibrium with the liquid composition and all of the heat flux results in evaporation at the interface. Also, it is postulated that mass transfer has no effect on the heat transfer coefficient but affects the thermal driving force. A ratio of the thermal driving force for a binary mixture to the single-component driving force is introduced to account for the reduction in heat transfer. A modified Reynolds analogy is used to take into account the Prandtl number effect. In developing the present model, the Bennett-Chen correlation is implemented for the saturated boiling region.

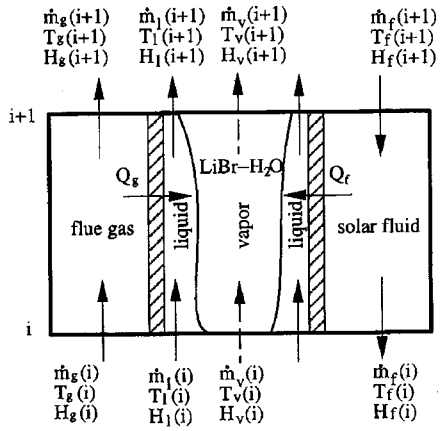

Fig. 3 Control volume for an incremental section

Analysis for Region I. Figure 3 shows a control volume for which mass and energy balances are established. Since this is the subcooled region for the water-lithium bromide liquid, no phase change is involved and the vapor mass flow rate is zero.

Mass conservation:

$$\dot{m}_g(i) = m_l(i+1) \tag{1}$$

$$\dot{m}_f(i) = m_g(i+1) \tag{2}$$

$$\dot{m}_l(i) = \dot{m}_f(i+1) \tag{3}$$

Energy conservation:

$$\dot{m}_g(i)H_g(i) = \dot{m}_g(i+1)H_g(i+1) + Q_g(i) \tag{4}$$

$$\dot{m}_f(i)H_f(i) = \dot{m}_f(i+1)H_f(i) + Q_f(i) \tag{5}$$

$$\dot{m}_l(i)H_l(i) = \dot{m}_l(i+1)H_l(i+1) + Q_g(i) + Q_f(i) \tag{6}$$

$Q_g(i)$ and $Q_f(i)$ are determined from heat transfer equations

$$Q_g(i) = (U\Delta A)_g(\mathrm{LMTD})_g \tag{7}$$

$$Q_f(i) = (U\Delta A)_f(\mathrm{LMTD})_f \tag{8}$$

where U_g and U_f are local overall heat transfer coefficients for the flue gas and solar fluid, respectively. ΔA represents the incremental area. The log mean temperature differences $(\mathrm{LMTD})_g$ and $(\mathrm{LMTD})_f$ are defined as

$$(\mathrm{LMTD})_g = \frac{[T_g(i+1) - T_l(i+1)] - [T_g(i) - T_l(i)]}{\ln\left[\dfrac{T_g(i+1) - T_l(i+1)}{T_g(i) - T_l(i)}\right]} \tag{9}$$

$$(\mathrm{LMTD})_f = \frac{[T_f(i+1) - T_l(i+1)] - [T_f(i) - T_l(i)]}{\ln\left[\dfrac{T_f(i+1) - T_l(i+1)}{T_f(i) - T_l(i)}\right]} \tag{10}$$

The flow on the flue gas side is normally laminar and the heat transfer coefficient is calculated as for flow in a rectangular duct or between parallel plates, depending on the duct aspect ratio [6]. The solar fluid is flowing inside the fluted tubes with no phase change. Its heat transfer coefficient is obtained by applying the single-phase heat transfer correlations developed by Srinivasan and Christensen [7].

$$\mathrm{Nu}_f = 0.014\,\mathrm{Re}^{0.842}e^{*-0.067}p^{*-0.293}\theta^{*-0.705}\mathrm{Pr}^{0.4}$$
$$(500 < \mathrm{Re} < 5000) \tag{11}$$

$$\mathrm{Nu}_f = 0.064\,\mathrm{Re}^{0.773}e^{*-0.242}p^{*-0.108}\theta^{*0.599}\mathrm{Pr}^{0.4}$$
$$(5000 < \mathrm{Re} < 80000) \tag{12}$$

Downloaded From: https://energyresources.asmedigitalcollection.asme.org on 06/28/2019 Terms of Use: http://www.asme.org/about-asme/terms-of-use

The water-lithium bromide solution flows around the annulus side of the fluted tubes. As it heats up, its temperature increases until it reaches the saturation temperature corresponding to the solution concentration and pressure, which marks the end of the region I. The heat transfer coefficient for the single-phase heat transfer of the LiBr-H_2O is calculated using correlations developed at Ohio State University [8]

$$f=\frac{96r^{*0.035}}{\mathrm{Re}}(1+101.7\,\mathrm{Re}^{0.52}e^{*(1.85+\theta^*)}r^{*5.77}) \tag{13}$$

$$f=4\left[1.7372\ln\left(\frac{\mathrm{Re}}{1.964\ln(\mathrm{Re})-3.8215}\right)\right]^{-2}(1+0.0925r^*)\times(1+222\,\mathrm{Re}^{0.09}e^{*2.4}p^{*-0.49}\theta^{*-0.34}r^{*2.22}),\quad(\mathrm{Re}>800) \tag{14}$$

$$\mathrm{Nu}_{1-\phi}=\frac{f}{8}\frac{\mathrm{Re\,Pr}}{1+9.77\sqrt{f/8}(\mathrm{Pr}^{2/3}-1)}\mathrm{Re}^{-0.2}\times e^{*-0.32}p^{*-0.28}r^{*-1.64} \tag{15}$$

Analysis for Region II. Since the refrigerant is pure water, the vapor does not contain any lithium bromide. This observation simplifies the mass balance equations.

Mass balance:

$$\dot{m}_g(i)=\dot{m}_g(i+1) \tag{16}$$

$$\dot{m}_f(i)=\dot{m}_f(i+1) \tag{17}$$

$$\dot{m}_l(i)+\dot{m}_v(i)=\dot{m}_l(i+1)+\dot{m}_v(i+1) \tag{18}$$

Energy balance:

$$\dot{m}_g(i)H_g(i)=\dot{m}_g(i+1)H_g(i+1)+Q_g(i) \tag{19}$$

$$\dot{m}_f(i)H_f(i)=\dot{m}_f(i+1)H_f(i)+Q_f(i) \tag{20}$$

$$\dot{m}_l(i)H_l(i)+\dot{m}_v(i)H_v(i)=\dot{m}_l(i+1)H_l(i+1)+\dot{m}_v(i+1)H_v(i+1)+Q_g(i)+Q_f(i) \tag{21}$$

$Q_g(i)$ and $Q_f(i)$ are given by heat transfer

$$Q_g(i)=(U\Delta A)_g(\mathrm{LMTD})_g \tag{22}$$

$$Q_f(i)=(U\Delta A)_f(\mathrm{LMTD})_f \tag{23}$$

where

$$\frac{1}{(U\Delta A)_g}=\frac{1}{\eta_g h_g\Delta A_g}+\frac{\ln(D_o/D_i)}{2\pi k\Delta L}+\frac{1}{h_s\Delta A_s} \tag{24}$$

$$\frac{1}{(U\Delta A)_f}=\frac{1}{h_f\Delta A_f}+\frac{\ln(D_{vo}/D_{vi})}{2\pi k\Delta L}+\frac{1}{h_s\Delta A_s} \tag{25}$$

and

$$(\mathrm{LMTD})_g=\frac{[T_g(i+1)-T_l(i+1)]-[T_g(i)-T_l(i)]}{\ln\left[\dfrac{T_g(i+1)-T_l(i+1)}{T_g(i)-T_l(i)}\right]} \tag{26}$$

$$(\mathrm{LMTD})_f=\frac{[T_f(i+1)-T_l(i+1)]-[T_f(i)-T_l(i)]}{\ln\left[\dfrac{T_f(i+1)-T_l(i+1)}{T_f(i)-T_l(i)}\right]} \tag{27}$$

where h_g and h_f are the heat transfer coefficients on the flue gas side and the solar fluid side, respectively. They can be calculated in the same way as illustrated in region I. The heat transfer coefficient for the lithium bromide-water mixture undergoing forced convective boiling is h_s. Since only the water is desorbed from the solution and is the only component in the vapor phase, combined heat and mass transfer analysis in the vapor phase is avoided. But combined heat and mass transfer analysis is critical if more than one component exists in the vapor phase [9]. In that case, a concentration gradient is formed in the vapor phase due to the diffusion of different species. For instance, in an ammonia-water absorber or desorber, both the ammonia (the refrigerant) and the water (the solvent) exist in the vapor phase. The combined heat and mass transfer analysis determines the variation of the concentration of ammonia at the liquid-vapor interface and in the vapor. However, water-lithium bromide boiling differs from single-component boiling. Chen's modified forced convective boiling correlation [5] is applied in this study to account for the reduction in heat transfer coefficient due to the smaller thermal driving force for binary mixtures. Chen's correlation is divided into two parts: for microscopic heat transfer (nucleate boiling) and macroscopic heat transfer (bulk forced convection). The overall heat transfer coefficient is the summation of both

$$h_f=h_{nb}S_{\mathrm{binary}}+h_{fc}F_{\mathrm{binary}} \tag{28}$$

$$h_{nb}=0.00122\frac{k_l^{0.79}c_{pl}^{0.45}\rho_l^{0.49}}{\sigma^{0.5}\mu_l^{0.29}h_{fg}^{0.24}\rho_v^{0.24}}(\Delta T_{\mathrm{sat}})^{0.24}(\Delta p_{\mathrm{sat}})^{0.75} \tag{29}$$

where

$$S_{\mathrm{binary}}=\frac{1}{1-\dfrac{C_{pl}(x_v-x_l)}{h_{fg}}\left.\dfrac{\partial T_{\mathrm{sat}}}{\partial x_l}\right|_p\left(\dfrac{\alpha}{D_{ij}}\right)^{1/2}}S \tag{30}$$

$$S=\frac{1}{1+2.53\times10^{-6}(\mathrm{Re}_lF^{1.25})^{1.17}} \tag{31}$$

$$F_{\mathrm{binary}}=\left[\frac{\mathrm{Pr}_l+1}{2}\right]^{0.444}\left[1-\frac{(1-x_v)\dot{q}}{\rho_{\mathrm{avg}}h_{fg}h_m\Delta T}\left.\frac{\partial T_{\mathrm{sat}}}{\partial x_l}\right|_p\right]F \tag{32}$$

$$F=\begin{cases}1 & \dfrac{1}{X_{tt}}<0.1\\[2ex] 2.35\left(0.213+\dfrac{1}{X_{tt}}\right)^{0.736} & \dfrac{1}{X_{tt}}>0.1\end{cases} \tag{33}$$

$$\frac{1}{X_{tt}}=\left(\frac{\mu_v}{\mu_l}\right)^{0.1}\left(\frac{y}{1-y}\right)^{0.9}\left(\frac{\rho_l}{\rho_v}\right)^{0.5} \tag{34}$$

where S_{binary} is the suppression factor for the binary mixture, the factor F_{binary} accounts for the enhanced flow and turbulence due to the presence of vapor, X_{tt} is the Lockhart-Martinelli parameter, and h_{fc} is the single-phase forced convective heat transfer coefficient based only on the liquid mass flow rate and is calculated using Eqs. (13)–(15).

Design Procedures. If the solar energy is sufficient to drive the generator, the generator operates with only the solar energy supply. However, if solar energy is not available or insufficient, supplementary gas heat has to be used to fire the generator. Therefore, the generator might be powered by solar fluid together with supplementary flue gas. In this case, the energy balances have to be satisfied for the water-lithium bromide, the flue gas, and the solar fluid simultaneously. In the design process, two iterations enforce the energy balances for all fluids involved. The heat transfer mechanism in the single-phase flow region is different from that in the two-phase flow region; hence, different design procedures were adopted for each region. The design procedures are outlined as follows:

Region I

1 Calculate T_{sat} at the given inlet solution concentration and pressure.
2 Set an incremental length ΔL.
3 Calculate the thermodynamic and transport properties based on the local temperature and concentration.
4 Calculate heat transfer coefficients h_g and h_f.

Downloaded From: https://energyresources.asmedigitalcollection.asme.org on 06/28/2019 Terms of Use: http://www.asme.org/about-asme/terms-of-use

5 Guess an incremental temperature ΔT_s, $T_s(i+1)=T_s(i)+\Delta T_s$.
6 Calculate enthalpy $H_l(i+1)$ and total heat transfer rate added to the water-lithium bromide solution $Q(i)=Q_g(i)+Q_f(i)$ based on the energy balance.
7 Calculate heat transfer coefficient h_s.
8 Guess ΔT_f, $T_f(i+1)=T_f(i)+\Delta T_f$.
9 Calculate $Q_f=\dot{m}_f C_{p_f}(T_f(i+1)-T_f(i))$ and $(\mathrm{LMTD})_f$.
10 Calculate $Q_f'=(U\Delta A)_f(\mathrm{LMTD})_f$.
11 If $|(Q_f-Q_f')/Q_f|>10^{-3}$, go back to step 8 and choose a new ΔT_f. Otherwise, continue.
12 Calculate $Q_g(i)=Q(i)-Q_f(i)$ and

$$T_g(i+1)=T_g(i)-\frac{Q_g(i)}{\dot{m}_g C_{p_g}}.$$

13 Calculate $(\mathrm{LMTD})_g$ and $Q_g'=(U\Delta A)_g(\mathrm{LMTD})_g$.
14 If $|(Q_g-Q_g')/Q_g|>10^{-3}$, go back to step 5 and choose a new ΔT_s. Otherwise, continue.
15 Compare $T_s(i+1)$ with T_{sat}. If $T_s(i+1)<T_{\mathrm{sat}}$, march to the next segment by setting $i=i+1$ and go back to step 3. Otherwise, go to region II.

Region II

16 Calculate the thermodynamic and transport properties including water vapor properties at local temperatures.
17 Calculate heat transfer coefficients h_g and h_f.
18 Guess an incremental liquid concentration of lithium bromide Δx_l, $x_l(i+1)=x_l(i)+\Delta x_l$.
19 Calculate $T_s(i+1)$ based on $x_l(i+1)$.
20 Calculate $\dot{m}_l(i+1)$ and $\dot{m}_v(i+1)$ based on mass balance.
21 Calculate enthalpies $H_l(i+1)$ and $H_v(i+1)$ based on $T_s(i+1)$ and $x_l(i+1)$.
22 Calculate total heat transfer rate added to the water-lithium bromide mixture $Q(i)=Q_g(i)+Q_f(i)$ based on the energy balance.
23 Calculate Lockhart-Martinelli parameter, suppression factor and enhancement factor.
24 Calculate forced convective heat transfer coefficient h_{fc}.
25 Guess wall temperature $T_w(i)$.
26 Calculate the nucleate boiling heat transfer coefficient h_{nb}.
27 Guess ΔT_f, $T_f(i+1)=T_f(i)+\Delta T_f$ and calculate $Q_f=\dot{m}_f Cp_f(T_f(i+1)-T_f(i))$.
28 Calculate $(\mathrm{LMTD})_f$ and $Q_f'=(U\Delta A)_f(\mathrm{LMTD})_f$.
29 If $|(Q_f-Q_f')/Q_f|>10^{-3}$, go back to step 27 and choose a new ΔT_f. Otherwise, continue.
30 Calculate $Q_g(i)=Q(i)-Q_f(i)$ and $T_g(i+1)=T_g(i)-Q_g(i)/(\dot{m}_g C_{pg})$.
31 Calculate wall temperature $T_w'(i)$ based on newly obtained heat transfer rates and heat transfer coefficients.
32 If $|(T_w(i)-T_w'(i))/T_w(i)|>10^{-3}$, set $T_w(i)=0.5\times(T_w(i)+T_w'(i))$ and go back to step 26. Otherwise, continue.
33 Calculate $(\mathrm{LMTD})_g$ and $Q_g'=(U\Delta A)_g(\mathrm{LMTD})_g$.
34 If $|(Q_g-Q_g')/Q_g|>10^{-3}$, go back to step 18 and choose a new Δx_i. Otherwise, continue.
35 Calculate cumulative heat transfer rate

$$Q_{\mathrm{cumulative}}=\sum_{j=1}^{i} Q(j).$$

36 Compare $Q_{\mathrm{cumulative}}$ with the required heat duty for the generator Q_{required}. If $Q_{\mathrm{cumulative}}<Q_{\mathrm{required}}$, march to the next segment by setting $i=i+1$ and go back to step 16. Otherwise, stop.

Results and Discussion

1 Solar Energy Serves as the Only Driving Energy. Figure 4 shows the temperature profile for the generator when solar energy is the only driving energy. The horizontal axis represents the percentage of the generator length. As can be seen, the solar fluid and the water-lithium bromide solution are in countercurrent flow. The water-lithium bromide solution is subcooled at the inlet of the generator. As it is heated up by the hot solar fluid, its temperature gradually approaches the saturation temperature specified by the solution concentration and pressure. The length of region I is roughly 44 percent of the total length. The heat transfer rate for region I is $Q_{\mathrm{I}}=12.03$ kW, and the heat transfer rate for region II is $Q_{\mathrm{II}}=47.58$ kW. Although the length of the region I is 44 percent of the total length, it only delivers about 20 percent of the total heat load. This is because single-phase heat transfer occurs in this region. The solution side heat transfer coefficient in this region ranges from 641.6 W/m^2-K to 689.9 W/m^2-K. The heat transferred from the solar fluid to the water-lithium bromide solution, Q_{I}, is to heat the solution to the saturation temperature.

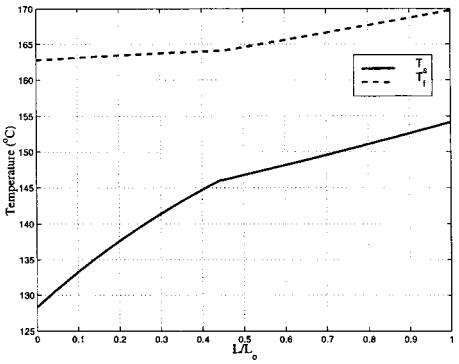

Fig. 4 Temperature profile for generator solely powered by solar energy

On the other hand, the solution side heat transfer coefficient for region II ranges from 4451 W/m^2-K to 6180.4 W/m^2-K, which is about seven times higher than that for region I. It is the phase change in region II that gives rise to the high heat transfer coefficient. Nearly 80 percent of the total heat transfer occurs in region II, which occupies 56 percent of the total length. It is evident that the subcooling of the water-lithium bromide solution has a significant impact on the size of the generator. As the degree of subcooling drops, the generator size will decrease considerably.

The solution temperature increases as it flows toward the exit because the water is being desorbed from the solution, which results in a higher LiBr concentration for the liquid phase. The higher liquid concentration corresponds to the higher saturation temperature. The temperature difference between the solution side and the solar fluid side decreases along the length of the heat exchanger. The pinch point of 15.6°C occurs at the inlet of the solar fluid. The generator size is very sensitive to the solar fluid inlet temperature. For instance, if the solar fluid temperature is raised from 170°C (as given in the foregoing) to 173°C, the actual length of the generator will decrease by 14 percent for the same amount of heat load and the same target exit solution temperature and concentration.

2 Flue Gas Serves as the Only Driving Energy. The generator can be fired by only natural gas if solar energy is not available (cloud cover or after dark). To enhance the heat transfer on the gas side, rectangular fins are used downstream of the gas flow to cover 29 percent of the total length. Figure 5 shows the temperature profiles when the generator is fired only by flue gas. Figure 5(*a*) shows the temperature distribution for both the water-lithium bromide solution and the flue gas, while Fig. 5(*b*) shows only the solution temperature on an enlarged scale.

The flue gas and the water-lithium bromide solution are in cocurrent flow and the temperatures of these two fluids approach each other as they move closer to the exit. The flue gas temperature drops quickly in the section with rectangular fins due to the increased heat transfer area and the higher heat transfer coefficient. In the section without fins, the heat transfer coefficient starts

Downloaded From: https://energyresources.asmedigitalcollection.asme.org on 06/28/2019 Terms of Use: http://www.asme.org/about-asme/terms-of-use

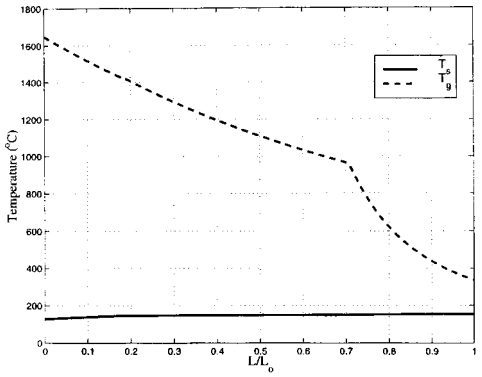

(*a*)

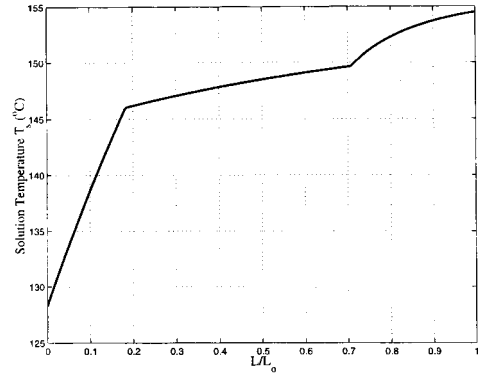

(*b*)

Fig. 5 Temperature profiles as generator fired only by flue gas

from 61.32 W/m^2-K at the inlet and gradually drops to 41.91 W/m^2-K at the end of the section. With the introduction of the rectangular fins, the heat transfer coefficient increases to 84.04 W/m^2-K, more than double the degraded heat transfer at the end of the unfinned section. At the end of the rectangular fin section, the heat transfer coefficient is about 42.98 W/m^2-K. The enhanced heat transfer due to the rectangular fins also results in a more rapid increase in the solution temperature in the finned section as shown in Fig. 5(*b*). Although the rectangular fin section occupies only 29 percent of the total length, it contributes nearly 43 percent of the total heat transfer.

Another observation is that the single-phase region for this case is much shorter than that for the solar energy driven mode. The length of the region I is about 18 percent of the total length of the generator and the cumulative heat transfer rate for this region is about 20 percent of the total heat transfer rate, proportionate to its length. This is clearly different from that for the solar energy-driven mode discussed in the foregoing. In the flue gas-driven generator, the water-lithium bromide solution temperature swiftly reaches the saturation point after it enters the generator as a subcooled liquid. Such behavior is the result of the enormous temperature difference between the flue gas and the solution.

Figure 6 illustrates the variation of the concentration of water-lithium bromide mixture along the generator. In region I, the concentration remains constant since there is no desorption of water. However, the concentration starts to increase as the boiling initiates in region II. Region II is divided into two sections, with or without fins. Greater heat transfer in the finned section causes the solution temperature to increase rapidly, facilitating the desorption of the water from the liquid solution much more quickly than in the unfinned section. Therefore, a greater increase in concentration is observed in the finned section.

3 Dual-Fired Mode. When the solar energy is only able to provide part of the heat requirement of the generator, natural gas is utilized as the supplementary heat source. The amount of energy needed from natural gas is determined not only by the solar fluid inlet temperature and flow rate, but also by the actual configuration of the generator. The total length of the generator and the length of the finned section are important in determining the gas exit temperature and the burner efficiency. Figure 7 shows a typical temperature distribution in the generator fired by natural gas and solar fluid simultaneously. In this example, the solar fluid flow rate is 1.26 kg/s compared to the flow rate of 2.05 kg/s when the solar fluid is used exclusively. The solar fluid inlet temperature is 170°C, which is the same as before. The supplementary flue gas flow rate is 0.00756 kg/s. In this case, the flue gas exit temperature is about 196°C. Figure 7(*a*) gives all the temperature

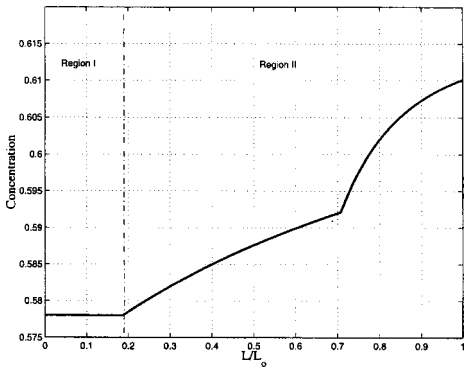

Fig. 6 Concentration profile as generator is powered only by flue gas

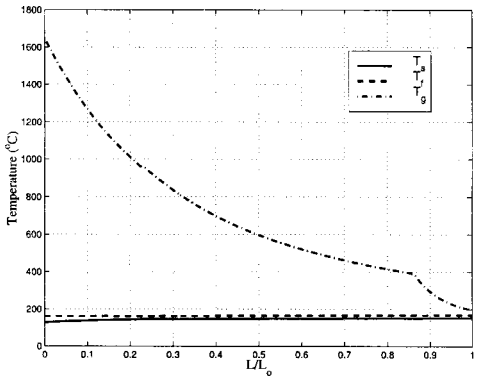

(*a*)

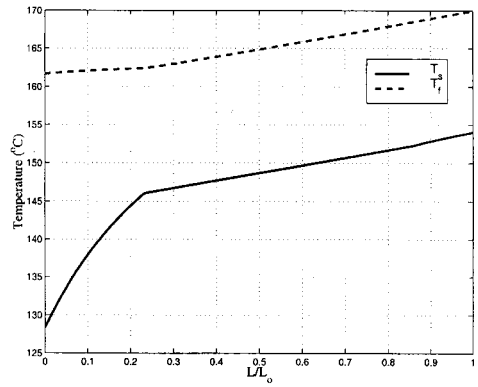

(*b*)

Fig. 7 Temperature profiles for the generator powered by flue gas and solar fluid

Downloaded From: https://energyresources.asmedigitalcollection.asme.org on 06/28/2019 Terms of Use: http://www.asme.org/about-asme/terms-of-use

Table 4 Computational results for the dual-fired generator

Gas flow rate m_g (kg/s)	Solar fluid flow rate m_f (kg/s)	Solar fluid inlet temperature $T_{f,\,inlet}$ (°C)	Gas exit temperature $T_{g,exit}$ (°C)
0.00630	1.638	170	194
0.00756	1.638	170	288
0.00756	1.260	170	196
0.00882	1.260	170	248
0.00945	1.260	170	307
0.00945	0.882	170	175

profiles for the flue gas, solar fluid and aqueous lithium bromide, while Fig. 7(*b*) only shows the solar fluid and aqueous lithium bromide temperatures on an enlarged scale.

Table 4 provides some results showing how flow rates of the solar fluid and flue gas affect the flue gas exit temperature. In the calculation, the total heat duty of the generator for each case is kept the same, and the finned section always starts at the same position, 0.762 m above the burner. The solar fluid inlet temperature is maintained at 170°C in all cases. Therefore, the overall size of the generator may vary with each case. In other words, for a given solar fluid flow rate, flue gas flow rate, solar fluid inlet temperature and total heat duty, the generator size is a calculated value. It can be seen from Table 4 that the flue gas exit temperature increases if the flue gas flow rate increases when the solar fluid flow rate is constant. The flue gas exit temperature drops as the solar fluid flow rate decreases if the flue gas flow rate is constant. The optimal flue gas flow rate for a given solar fluid inlet temperature, concentration and flow rate should be based on the acceptable flue gas exit temperature.

Experimental Results

Two 25RT dual-fired generators were fabricated based on the foregoing modeling results. These generators were installed with a commercial 50RT water-lithium bromide absorption chiller that has COP ($=Q_{evap}/Q_{input}$) of 1.0. Detailed experimental investigation including experimental equipment and procedures will be reported in another paper. Experimental results demonstrated that the generators yield satisfactory performance. Table 5 shows the experimental results when the generators are in gas-fired mode. Target value indicates the operating condition specified in the original chiller design. Table 6 illustrates the experimental results when the generators are fired by steam. It should be noted that the generators are designed for hot water and/or gas fired according to our model; but the experiment was conducted using steam as a substitute for hot water. Therefore, the comparison is not strictly valid for steam-fired mode. Nonetheless, the steam-fired generators exhibit very good performance, which gave us much confidence in the hot water-fired mode. The hot water test will be performed in the future field test when the solar collector array is set up. Table 7 presents the chiller performance when the generators were fired by gas and steam simultaneously.

Table 5 Experimental results of chiller performance as the generators are fired by gas

	Target Value	Experimental Result
Chilled water inlet temperature (°C)	-	12.8
Chilled water exit temperature (°C)	7	7.8
Chilled water flow rate (kg/min)	458	489
Cooling water inlet temperature (°C)	29.4	26.3
Cooling water flow rate (kg/min)	765	698
Flue gas heat input (kW)	175.9	168.9
Cooling capacity (RT)	50	49
COP	1.0	1.05

Table 6 Experimental results of chiller performance as the generators are fired by steam

	Target Value	Experimental Result
Chilled water inlet temperature (°C)	-	13.7
Chilled water exit temperature (°C)	7	7.9
Chilled water flow rate (kg/min)	458	494
Cooling water inlet temperature (°C)	29.4	26.8
Cooling water flow rate (kg/min)	765	682
Steam flow rate (kg/min)	-	4.33
Steam temperature (°C)	-	158.3
Cooling capacity (RT)	50	56
COP	1.0	1.31

Table 7 Experimental results of chiller performance as the generators are fired by steam and gas

	Experimental Result
Chilled water inlet temperature (°C)	13.9
Chilled water exit temperature (°C)	8.6
Chilled water flow rate (kg/min)	484
Cooling water inlet temperature (°C)	26.6
Cooling water flow rate (kg/min)	700
Flue gas heat input (kW)	85.2
Steam flow rate (kg/min)	2.24
Steam temperature (°C)	147.8
Cooling capacity (RT)	51
COP	1.10

Summary

This paper presents a design procedure for a dual solar/gas-fired water-lithium bromide generator and some design results. The generator is divided into two different regions according to the heat transfer mechanism. The reduction of heat transfer coefficient due to the binary mixture boiling has been considered by using Bennett-Chen's correlation. Simultaneous solar and gas-fired desorption has been investigated. The design procedure has been implemented in a computer model and presents reasonable results.

Nomenclature

A = area (m^2)
C_p = specific heat capacity (J/kg-K)
D_b = bore diameter for fluted tube (m)
D_e = envelope diameter for fluted tube (m)
D_v = volumetric diameter (m)
D_{ij} = mass diffusion coefficient (m^2/s)
e^* = nondimensional flute height
f = friction factor
F = enhancement factor
H = enthalpy (J/kg)
h = heat transfer coefficient (W/m^2-K)
k = conductivity (W/m-K)
L = length (m)
L_o = true total length of generator (m)
L^* = nondimensional length, L/L_o
LMTD = log mean temperature difference (°C)
$\dot{m}$ = mass flow rate (kg/sec)
N_s = number of starts of fluted tube
Nu = Nusselt no.
p = pressure (Pa)
p^* = nondimensional pitch
Pr = Prandtl no.
Q = heat transfer rate (W)

Downloaded From: https://energyresources.asmedigitalcollection.asme.org on 06/28/2019 Terms of Use: http://www.asme.org/about-asme/terms-of-use

$\dot{q}$ = heat flux (W/m^2)
r^* = radius ratio, $D_{vo}/D_{o,i}$
Re = Reynolds no.
S = suppression factor
T = temperature (°C)
t = thickness (m)
U = overall heat transfer coefficient (W/m^2-K)
x = mass fraction of lithium bromide
X_n = Lockhart-Martinelli parameter
y = vapor quality
α = thermal diffusivity (m^2/s)
η = overall fin efficiency
μ = dynamic viscosity (kg/m-s)
ρ = density (kg/m^3)
σ = surface tension (N/m)
θ^* = nondimensional flute helix angle

Subscripts

avg = average
evap = cooling capacity from evaporator
f = solar fluid
fc = forced convection
g = flue gas
i = inside
input = heat input to the generators
l = liquid
nb = nucleate boiling
o = outside, total length on L
s = water-lithium bromide solution
sat = saturation
v = vapor
w = wall

References

[1] ASHRAE, 1997, Handbook, Fundamentals, IP Edition. p. 18.1.
[2] DeVault, R. C., 1988, ''DOE Absorption Programs Overview,'' *Proc. 2nd DOE/ORNL Heat Pump Conference*, pp. 104–109.
[3] Grossman, G., Gommed, K., and Gadoth, D., 1991, ''Computer Model for Simulation of Absorption Systems in Flexible and Modular Form,'' Final Report for Oak Ridge National Laboratory, Subcontract 90-89673.
[4] Taitel, Y., Bornea, D., and Dukler, A. E., 1980, ''Modeling Flow Pattern Transitions for Steady Upward Gas-Liquid Flow in Vertical Tubes,'' AIChE J., **26**, p. 345.
[5] Bennett, D., and Chen, J. C., 1980, ''Forced Convective Boiling in Vertical Tubes for Saturated Pure Components and Binary Mixtures,'' AIChE J., **26**, pp. 454–461.
[6] Shah, R. K., and London, H. L., 1978, ''Laminar Flow Forced Convection in Ducts,'' *Advances in Heat Transfer*, Supplement, Academic Press, New York, NY.
[7] Srinivasan, V., and Christensen, R. N., 1992, ''Experimental Investigation of Heat Transfer and Pressure Drop Characteristics of Flow through Spirally Fluted Tubes,'' Exp. Therm. Fluid Sci., **5**, pp. 820–827.
[8] The Ohio State University, 1993, ''A Manual for Heat Exchanger Design Using Spirally Fluted Tubes.''
[9] Kang, Y. T., and Christensen, R. N., 1993, ''Development of a Counter-Current Model for a Vertical Fluted Tube GAX Absorber,'' *Int. Absorption Heat Pump Conference Proc*.

Downloaded From: https://energyresources.asmedigitalcollection.asme.org on 06/28/2019 Terms of Use: http://www.asme.org/about-asme/terms-of-use